

Article

Investigation of Viscoelastic-Plastic Properties of Fresh Cemented Gangue Fly Ash Backfill Slurries

Yuxin Hao ^{1,*}, Xuepeng Song ¹, Chengshuai Wang ^{1,2}, Bowen Fan ¹ and Kai Yang ³

¹ School of Energy and Mining Engineering, China University of Mining and Technology (Beijing), Beijing 100083, China

² Shanxi Province Energy Vocational School, Taiyuan 030012, China

³ BGRIMM Technology Group, Beijing 102628, China

* Correspondence: haoyuxin@student.cumt.edu.cn; Tel.: +86-185-0048-3878

Abstract: In underground filling mining, freshly prepared cemented gangue-fly ash backfill (CGFB) slurries are typically piped into the gobs. The rheological properties of backfill slurry during pipeline transportation have a direct impact on the transportation characteristics, which in turn affect pipeline blockage and wear. In this paper, the rheological behavior and viscoelastic-plastic properties of CGFB during pipeline transportation are investigated. The effects of different solid content and cement content on resistivity were tested experimentally, and their viscoelasticity and plasticity were analyzed. The results show that with the increase in solid phase content and cement content, the viscosity, yield stress, and energy storage modulus of the materials showed an increasing trend. The viscosity and yield stress of the material both increased, reaching 32.77% and 51.22%, respectively. It was found by the dynamic shear test that in the low-strain region, the material showed a more significant elastic nature of the solid, while in the high-strain region, the viscosity of the material gradually increased. Cement has a substantially lower resistivity than fly ash and gangue, and with the increase in solid concentration, the resistivity of the material shows an increasing trend. With the increase in cement content, the resistivity generally shows a decreasing trend, but it should be noted that the resistivity change trend may tend to stabilize after the cement content exceeds 12%. The study's findings can aid in understanding the rheological properties of CGFB and its viscoelastic-plastic behavior during the underground filling and conveying process, which can provide a reference basis for research and application in related fields.



Citation: Hao, Y.; Song, X.; Wang, C.; Fan, B.; Yang, K. Investigation of Viscoelastic-Plastic Properties of Fresh Cemented Gangue Fly Ash Backfill Slurries. *Minerals* **2024**, *14*, 401. <https://doi.org/10.3390/min14040401>

Academic Editor: Mamadou Fall

Received: 12 March 2024

Revised: 6 April 2024

Accepted: 12 April 2024

Published: 14 April 2024



Copyright: © 2024 by the authors. Licensee MDPI, Basel, Switzerland. This article is an open access article distributed under the terms and conditions of the Creative Commons Attribution (CC BY) license (<https://creativecommons.org/licenses/by/4.0/>).

Keywords: cemented gangue-fly ash backfill; viscoelastic-plastic properties; storage modulus; loss modulus; electrical resistivity

1. Introduction

As one of the most significant fossil energy sources in industry, coal is crucial to the social and economic advancement of people in the majority of the world's nations [1]. With the development of the economy, the energy consumption of human beings has increased, and more and more coal needs to be mined [2]. Coal mining serves as one of the major basic industries. Compared with other countries in the world, coal accounts for more than 50% or more of China's energy supply, but more than ninety percent of China's coal comes from underground mining [3–5]. The underground mining of coal causes surface subsidence and also produces a large amount of waste such as coal gangue, which causes serious pollution to the ecological environment [6]. At the same time, the more constrained space such as the working face roadway in the mining airspace is prone to accidents due to air leakage [7], so it is necessary to fill and seal the areas with higher constraint requirements such as the airspace or the working face roadway in the production process of coal mines to ensure that the coal mining is carried out safely [8,9].

In recent years, CGPB mixtures have been used for ground control and gangue waste disposal in underground coal mining operations [10]. CGFB, prepared using a mixture

of cement, gangue, fly ash, and water, is transported through boreholes and pipelines to underground mining areas [11–13]. This method not only controls subsidence but also reduces the emission accumulation of hazardous wastes (coal gangue) on the surface, thus solving the environmental safety problems associated with it (spontaneous burning of stacks of coal gangue and pollution by fly ash dust) to a certain extent [14]. During the filling process of CGFB, it is necessary to ensure that the CGFB slurry is efficiently transported to the designated area without pipeline clogging, which requires the CGFB slurry to have smooth transportability [15]. The rheological parameters of the slurry are influenced by its chemistry (binder hydration), hydraulics (suction development), and other factors [16,17]. Due to the makeup of CGFB, the binders used (cement) react chemically with water, also known as binder hydration, producing hydration products and consuming water [18]. The consumption of water leads to a reduction in pore water pressure or the development of suction inside the CGFB, which is macroscopically manifested by the slurry reflecting different visco-plasticity during the flow process. The traditional filling slurry test mostly focuses on the steady-state visco-plasticity test of the slurry, but there are interactions between the slurry and the pipe wall during the flow process, and the slurry also shows contact during the internal flow process. Moreover, the material will show viscoelasticity when encountering the unsteady flow state, which is specifically expressed as the impact on the pipe and the particle collision between the slurry, so it is necessary to assess the fresh slurry's viscoelastic plasticity shown in the flow process. Therefore, it is necessary to study the viscoelasticity of fresh slurry in the flow process.

Electrical resistivity (ER) is an important means of studying the properties of cementitious materials, which represents the ability of a material to resist the flow of current per unit length in a given cross-section [19–21]. This method can reflect changes in the internal structure of the material (number of pore structures and tortuosity, pore solution saturation, etc.) [22], is widely used in the study of cement–concrete materials and filled materials in terms of the coagulation process, monitoring of destabilization and damage processes, etc., and has the advantages of simplicity, rapidity, low cost, and non-destructive nature [23,24]. Resistivity testing, as a non-destructive measurement condition, can be a good test for internal reactions between materials. Hong Jae Yim et al. investigated non-destructive measurements such as resistivity to evaluate the microstructural evolution of fresh cement paste for 24 h and compared it with the setting time of the Vicat pin test. Observable non-destructive parameters, including setting time, can reflect the generation of cement hydrate and change the bending path of porous materials [25]. Xu Wenbin et al. proposed a non-destructive testing method to determine the mechanical properties of CPB using electrical resistivity (ER). Based on the logarithmic relationship with ER obtained at 90 days, the strength of CPB was developed to be evaluated using the resistivity testing method [26,27]. However, fewer studies have been conducted to characterize the viscoelasticity and plasticity of gangue fly ash slurries using resistivity.

This paper presents an experimental investigation into the fundamental aspects of CGFB and its rheological behavior, exhibiting viscoelasticity and plasticity. The resistivity of the material was also tested for different solids, cement contents, and times. The CGFB's characteristic flow curves and the fluctuating law of viscoelastic parameters were introduced and analyzed. The changing pattern of resistivity of the material was also analyzed to investigate the effect of concentration and cement content on the rheological properties of CGFB. The findings this paper presents are aimed at investigating the characterization of CGFB slurry rheological parameters to guide slurry pipeline transportation.

2. Materials and Methods

2.1. Materials

2.1.1. Gangue

During coal mining and washing, gangue emerges as the primary solid waste product. Gangue stone primarily consists of silicon and aluminum in addition to carbon since gangue and coal coexist together. It often results from oxidation and a few trace elements like

calcium, iron, sulfur, etc. [12]. Large particles are crushed by jaw crushers as filling slurry aggregate, gangue particle size by blasting action, coal mining machine cutting action, jaw crusher crushing action, etc. The maximum particle size of gangue particles crushed by jaw crushers is 0.01 m. The particle size distribution was measured using an OMIK LS-C (IIA) laser particle size analyzer, as shown in Figure 1. The chemical composition results are presented in Table 1. Gangue in the SiO₂ content of the highest 39.15%, Al₂O₃ followed by 26.38%, CaO content of 23.42%. The gangue also contains a small amount of Fe₂O₃. The gangue of this mine resembles claystone.

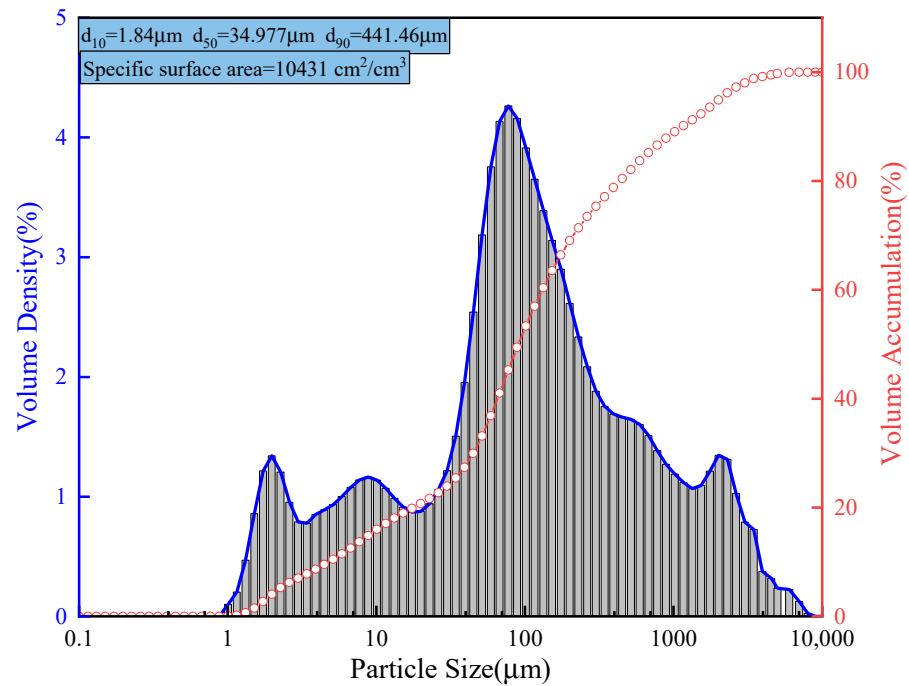


Figure 1. Particle size distribution of gangue.

Table 1. Major Chemical composition of gangue.

Chemical Composition	SiO ₂	Al ₂ O ₃	CaO	Fe ₂ O ₃	TiO ₂	K ₂ O	Total
Content	39.15	26.38	23.42	5.03	1.34	0.79	100

2.1.2. Fly Ash

Fly ash was obtained from the power plant near the mine. Measurements were made of the fly ash’s particle size, chemical makeup, and mineralogical composition. The density of the compacted fly ash was 1450 kg/m³. The particle size distribution is shown in Figure 2. The energy spectrum of the fly ash was analyzed using a HITACHIS-3500N scanning electron microscope. From Table 2, it can be seen that the content of SiO₂ in the fly ash was up to 57.68%, and the content of Al₂O₃ was 34.42%, Fe₂O₃ was 5.03%, and CaO was 1.42%, in addition to a small amount of K₂O, TiO₂, and Fe₂O₃ coexisting. The fly ash belongs to Class F in the experiment.

Table 2. Chemical composition of fly ash.

Chemical Composition	SiO ₂	Al ₂ O ₃	Fe ₂ O ₃	TiO ₂	K ₂ O	CaO	Total
Content	57.68	31.42	4.98	1.74	1.59	1.42	100

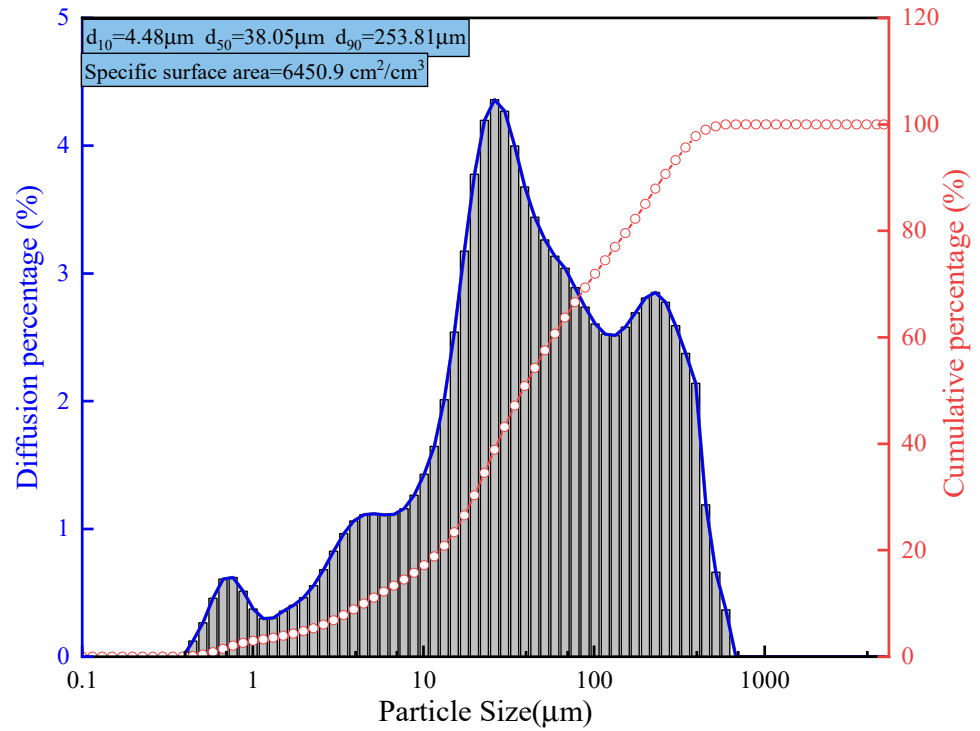


Figure 2. Particle size distribution of fly ash.

2.1.3. Binder

For the creation of CGFB blends, 425# ordinary silicate cement served as the binder, with a density of 3100 kg/m³. Its particle size distribution is shown in Figure 3, and its chemical composition is shown in Table 3.

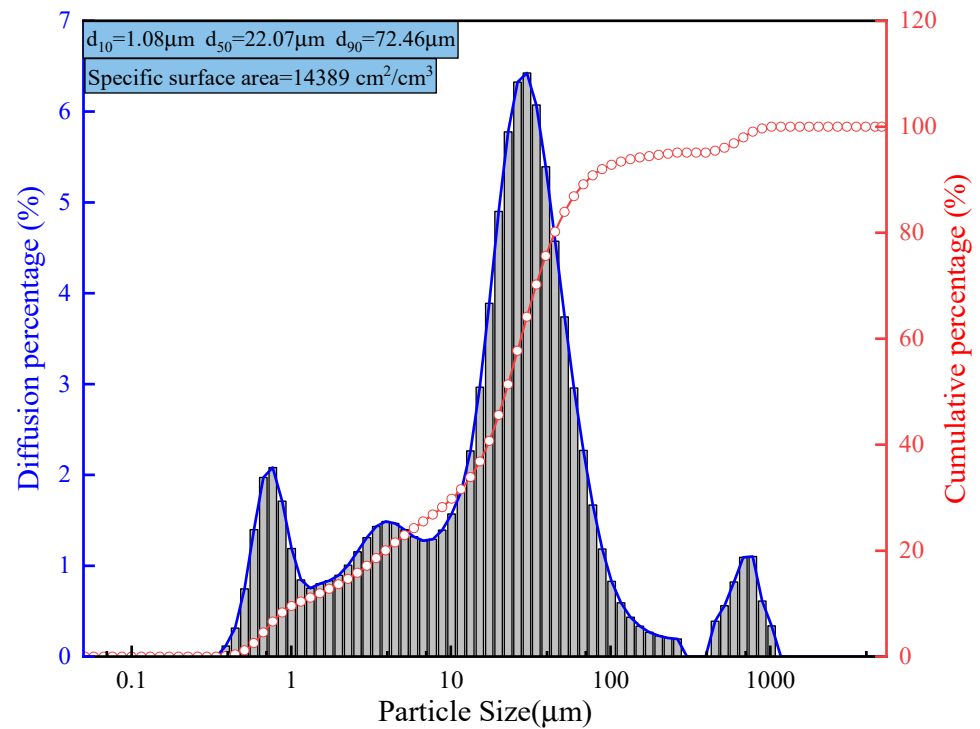


Figure 3. Particle size distribution of cement.

Table 3. Chemical composition of cement.

Chemical Composition	CaO	SiO ₂	Al ₂ O ₃	Fe ₂ O ₃	MgO	Others	Total
Content	64.55	23.28	5.42	3.48	1.19	2.08	100

2.1.4. Water

The binder and source material were mixed using deionized water. To create a mixture with the appropriate consistency, the volume of water was computed and measured.

2.2. Samples Preparation

The following experimental materials were weighed separately and added to a specific glass container: Crushed gangue, fly ash, cement, and water. Mix the mixture thoroughly for 5 min to blend and homogenize the gangue, fly ash, cement, and water to produce the desired CGFB mixture before rheological measurements. The dry mixture needs to be premixed in a beaker using a glass rod before adding water. Quantitatively weigh the water used and add it gradually to the mixing pot. A single speed (120 + 2 rpm) was used for the stirring process. In addition, it is necessary to observe the mixed slurry to ensure that the slurry in the container has been fully mixed and there is no dry mixture present. Every CGFB sample was made at the same room temperature (23 °C), and the detailed compositional ratios of the prepared mixtures are provided in Table 4.

$$w = \frac{M_c + M_g + M_f}{M_c + M_g + M_f + M_w} \times 100\%, \quad (1)$$

where w is the solids content concentration, M_d is the mass of desiccated raw material, and M_w is the mass of water. The dried materials include gangue, fly ash, and cement, thus allowing the equation:

$$w_c = \frac{M_c}{M_c + M_g + M_f} \times 100\%, \quad (2)$$

where M_c is the mass of cement, M_g is the mass of gangue and M_f is the mass of fly ash.

Table 4. Summary of the prepared CGFB slurry's component amounts.

Illustration of Nomenclature	SC72	SC73	SC74	SC75	SC76	CC8	CC10	CC12	CC14	CC16
w (%)	72	73	74	75	76	74	74	74	74	74
w_g (%)	58	58	58	58	58	64	62	60	58	56
w_f (%)	28	28	28	28	28	28	28	28	28	28
w_c (%)	14	14	14	14	14	8	10	12	14	16

The proportion of each in the solids is used to describe the cement content and fly ash content separately.

$$w_c = \frac{M_c}{M_c + M_g + M_f} \times 100\%, \quad (3)$$

$$w_f = \frac{M_f}{M_c + M_g + M_f} \times 100\%, \quad (4)$$

2.3. Apparatus and Experimental Procedures

2.3.1. Viscosity-Yield Stress Testing

As shown in Figure 4, the rheological parameters of fresh slurries were measured using a rate-controlled shear viscosity tester (Rheolab QC, Anton Paar, Graz, Austria). Concentric vane rotation is used to cause the slurry to move in a shear motion. The rheometer consists of a glass vessel for storing the slurry, and a rotating vane 20 mm from the bottom of

the glass vessel to mix the slurry in a shear motion, with a small enough gap so that the test material can withstand approximately uniform shear velocities. The gap between the bottom of the blade and the bottom of the glass vessel must be much larger than the maximum particle size of the material under test to give precise and representative measures of rheology. The inner vane has a radius of 21 mm, while the outer vessel has a radius of 50 mm. 700 g of sample was required for each test. To minimize the number of variables in the experiment, the temperature was maintained at 23 °C during the tests. After placing the slurry into a specific glass container, a computer program is initiated to control the rotation of the rotor. This test consists of two main phases. In stage I, the shear rate of the rheometer rotor is set to 100 r/s, thus allowing the slurry to be fully mixed. When stage I is completed, the rheometer rotor mixes the CGFB in a unidirectional linear incremental manner from 0 to 120 r/s in stage II. To determine the viscosity and yield stress of the slurry, the data from stage II are compiled, and the connection between the slurry's shear rate and shear stress is fitted into a curve [1]. In this paper, the impact of solids content and cement content on the rheological properties of CGFB was considered. In addition, the Bingham model is suitable for describing the rheological parameters of CGFB slurry, and its equation can be written as [28]:

$$\tau = \tau_0 + \eta \cdot \dot{\gamma} \quad (5)$$

where τ is shear stress, Pa; τ_0 is yield stress, Pa; η is plastic viscosity, Pa·s; $\dot{\gamma}$ is the shear rate, 1/s.

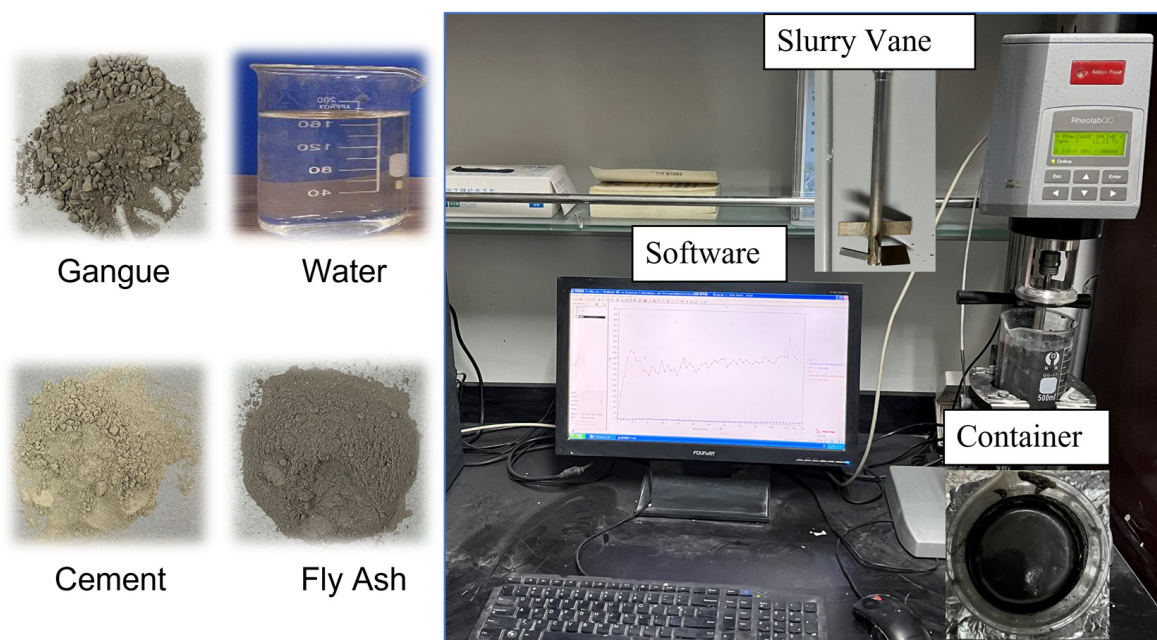


Figure 4. Raw materials and rheometer.

For the flow rates of CGFB slurry in pipelines, the shear rate can be calculated according to the hydraulic formula as follows:

$$\dot{\gamma} = \frac{8v}{D} \quad (6)$$

where $\dot{\gamma}$ is the shear rate experienced by the slurry during the flow process, Pa·s; v is the flow rate of the slurry [29].

2.3.2. Dynamic Shear Rheological Test

DSR dynamic shear rheometer (DHR-2, Waters, Milford, USA) was used to test the viscoelastic parameters of CGFB (Figure 5). The device consists of a rotor and parallel plates. It is connected to a computer for real-time data display, which can be tested to obtain the energy storage modulus and dissipation modulus that reflect the viscoelasticity of the material. The energy storage modulus reflects the energy stored in the material when it is subjected to force, which mainly reflects the elastic nature of the material. The dissipation modulus reflects the energy lost when a material is subjected to a force, mainly reflecting the viscous nature of the material. The energy storage modulus and dissipation modulus obtained from DSR testing can provide a reference for understanding the viscosity and yield stress of a material. A higher dissipation modulus usually implies a higher viscosity, while a higher energy storage modulus may be associated with a higher yield stress. Together, these parameters reveal the viscoelastic properties and rheological behavior of a material under stress, thus providing a comprehensive understanding of material properties. The steps for experimental testing are as follows: (1) Turn on the air compressor, confirm the pressure is about 3 bar, install the base for testing, plug in the data cable, and turn on the power of the rheometer main unit; (2) install the sample test plate, turn on the circulating water machine, and set the temperature at 23 degrees; (3) open the rheometer control software on the computer; (4) carry out self-check and calibration of the plate (plate inertia, air bearing friction correction); (5) add the sample to the fixture base, let the plate drop to clamp the sample, remove the excess sample, and keep the starting temperature equilibrium for 5 min; (6) set the test parameters for testing (first using the rotary mode, then the oscillation mode; the frequency of the oscillation mode is set to 1 Hz).

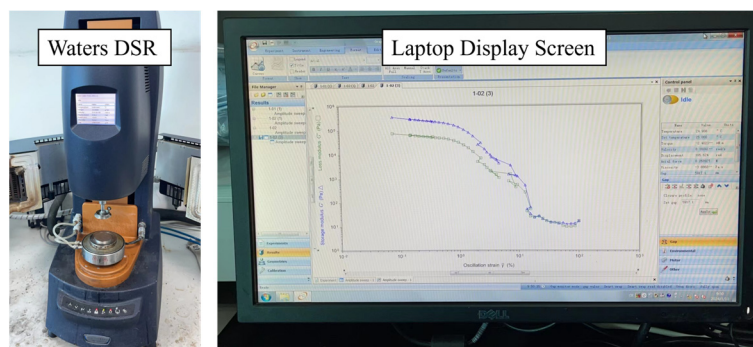


Figure 5. Dynamic shear rheometer.

2.3.3. Electrical Resistivity Test

Due to the poor conductivity of materials in solids, the relative value of resistivity can be obtained by diluting them in aqueous solution after treatment, which is the main way for ion exchange in water. In this study, a centrifugation-based resistivity testing method is proposed and tested using a Pentium Bente 321 resistivity tester (China). The test procedure is shown in Figure 6. The sieved materials were mixed according to the proportion using a mixer, and then 10 mL of deionized pure water was added, mixed again, and then put into a shaking box for shaking and mixing for 1 h. The well-mixed solution was put into the science high-speed centrifuge for centrifugation, and finally, the centrifuged material and the supernatant were obtained, and the electrodes of the calibrated resistivity tester were put into the measurement of the supernatant. The readings were taken every 5 min, and the test was carried out for 60 min for each group of materials. The resistivity of the three raw materials in water was first obtained. The resistivity test procedure is:

1. Clean the ORP electrode with distilled or deionized water.
2. Immerse the electrode sensor in the sample and stir slowly.
3. When the measured value stabilizes, the screen automatically displays the stable icon.
4. Record the measured value and the measurement is complete.



Figure 6. Resistivity testing equipment and steps.

Use the same procedure to test the resistivity of SC72-SC76 and CC8-CC16 group materials.

3. Results and Analysis

3.1. Visco-Plastic Test Results

3.1.1. Solid Content Effect

The relationship between shear rate and shear stress, as well as the relationship curve between shear rate and apparent viscosity, are collectively referred to as typical flow curves [30]. This paper focuses on the effects of concentration and cement content on the yield stress and viscosity of CGFB pastes through experiments. The unidirectional rates of the pastes were scanned. The experimental data were then averaged after each set of experiments was run three times [31]. The rheological characteristic curves of the pastes were analyzed by linear regression using data analysis software. Figure 7 illustrates the proven functional connection between shear rate and shear stress (example: sc75). The functional relationship's linear regression findings between shear stress and shear rate are shown in Table 5. The viscosity describes the rate of response of the material to shear stress, i.e., the shear stress applied per unit shear rate. It can be seen from the Figure 8 that the viscosity of the slurry shows a nonlinear increasing trend as the concentration increases from 72% to 76%, with growth rates of 4.69%, 4.34%, 13.46%, and 7.15%, respectively, totaling a growth rate of 32.77%. The initial shear stress showed a similar trend, with growth rates of 7.29%, 10.14%, 7.29%, 19.18%, and a total growth rate of 51.22% as the concentration increased. This may be because as the solid content concentration increases, the water lubricating film's thickness falls, which makes the inter-particle linkages in CGFB closer and there are more direct interactions between the particles. As a result, during shearing, there is greater friction between the two solid particles, and it is harder for them to glide over one another. In cases of sufficient mixing, the gas contained in the water decreases, reducing the cement and increasing the frictional resistance between the fly ash and the cement and gangue. In addition, the concentration of particles in the slurry increases, which leads to an increase in the forces between the particles and, thus, an increase in the yield stress. The high concentration of particles builds up more densely, making the interaction between the particles more significant, thus increasing the overall stiffness of the slurry.

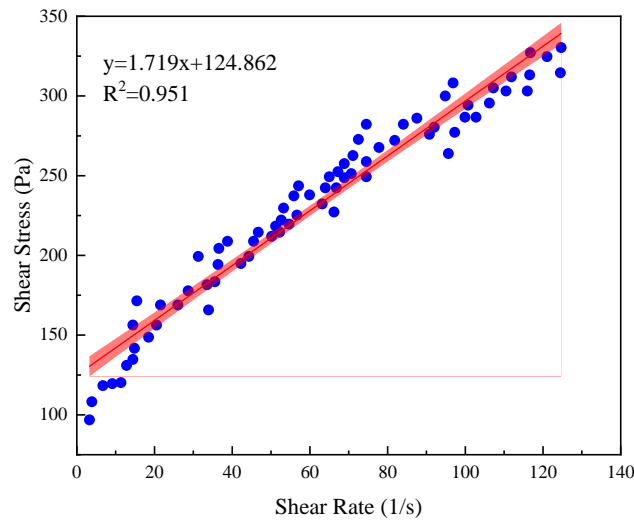


Figure 7. Relationship between shear stress and the shear rate of CGFB with a solid content of 75%.

Table 5. Shear rate and shear stress linear regression parameters.

Sample Nomenclature	Regression Equation	R ²	Yield Stress (Pa)	Viscosity (Pa·s)
SC72	1.387x + 98.463	0.971	98.463	1.387
SC73	1.452x + 105.631	0.983	105.631	1.452
SC74	1.515x + 116.365	0.968	116.365	1.515
SC75	1.719x + 124.862	0.951	124.862	1.719
SC76	1.842x + 148.791	0.958	148.791	1.842

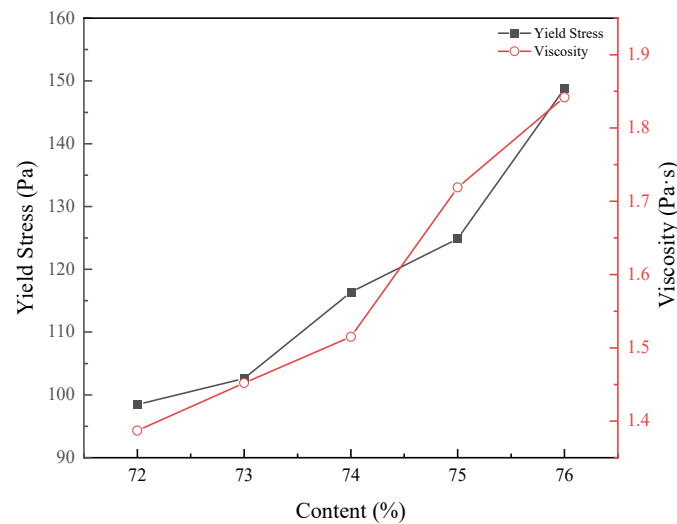


Figure 8. Viscosity and yield stress of slurry with solid content.

3.1.2. Cement Content Effect

Table 6 shows the variation of rheological parameters with cement content for the typical flow curve slurry of CGFB specimens with different cement dosages (8%, 10%, 12%, 14%, and 26%) under a fixed solid phase concentration. As seen in Figure 9, the cement content of gangue-filled slurry has an important influence on its rheological parameters. The viscosity and yield stress of the CGFB shows a nonlinear growth with the addition of more cement; the growth rate of viscosity is 13.10%, 12.95%, 21.67, and 15.70%, with a total growth rate of 79.78%; and the growth rate of yield stress is 10.16%, 8.64%, 15.32%, and 10.87%, with a total growth rate of 53.07%. The nonlinear growth of viscosity and yield

stress with the increase in cement content is related to the phenomenon of “flocculation” and the hydration reaction of the cement particles inside [32]. The flocculation phenomenon is manifested in the slurry with adsorbed water film of cement particles in the stirring effect of collision and contact, each other through the common adsorbed water film bonded together to form flocs, flocs are connected to form a loose mesh structure, and finally compacted under the action of gravity to form a three-dimensional floc structure that can resist deformation. The three-dimensional floc structure increases the difficulty of the flow of slurry, so that the slurry’s three-dimensional floc structure increases the difficulty of the slurry flow and increases the yield stress of the slurry. The more cement is mixed, the more significant the phenomenon of “flocculation into a group” inside the slurry, the greater the strength and stiffness of the floc structure, the greater the difficulty of slurry flow, and the greater the yield stress of the slurry. At the same time, the cement particles combined with the water hydration reaction consume the free water in the slurry, increasing the viscosity of the slurry. The higher the cement dosage, the more cement particles undergo hydration reactions per unit time, and the accumulation of particles and cement hydration products will affect the dynamic balance between “destruction” and “microstructure reconstruction” in the shear process to a certain extent [31]. In addition, the higher cement dosage leads to an increase in the average distance between CGFB particles, which is further exacerbated by particle collisions and subsequent particle clogging.

Table 6. Shear rate and shear stress linear regression parameters.

Sample Nomenclature	Regression Equation	R ²	Yield Stress (Pa)	Viscosity (Pa·s)
CC8	1.106x + 90.425	0.953	90.425	1.106
CC10	1.251x + 99.631	0.961	99.631	1.251
CC12	1.413x + 108.254	0.956	108.254	1.413
CC14	1.719x + 124.862	0.951	124.862	1.719
CC16	1.989x + 138.436	0.972	138.436	1.989

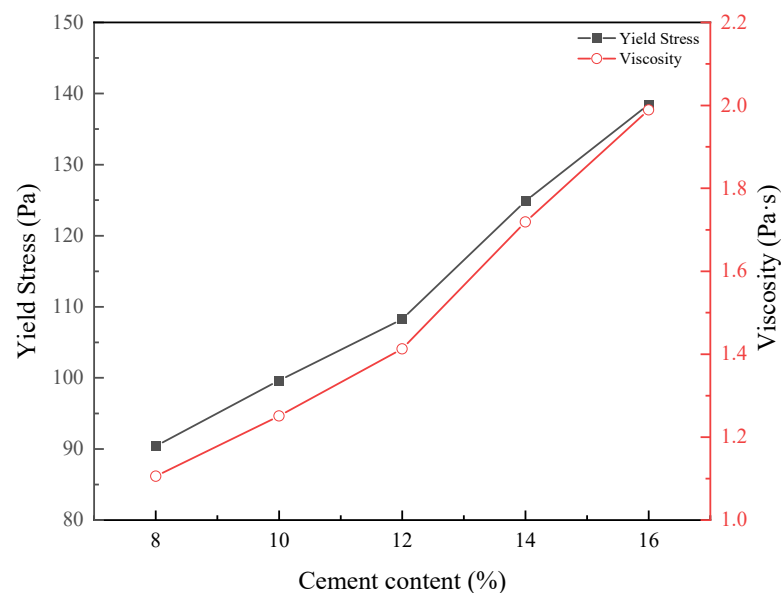


Figure 9. Rheological parameters of CGFB with different cement contents.

3.2. DSR Testing Results

The DSR test analysis of the CGFB slurry is shown in Figure 10, which demonstrates that the energy storage modulus and dissipation modulus of the material are in a decreasing condition as the oscillatory strain increases. In this paper, the oscillatory strain is categorized into three regions (low-strain, medium-strain, and high-strain regions). Taking Figure 10a

as an example, in the low-strain region, the energy storage modulus is larger than the dissipation modulus, and both the dissipation modulus and energy storage modulus decrease with increasing strain, which indicates that the elastic behavior of the material is more specific than viscous at this point. In the medium strain region, the energy storage modulus and dissipation modulus continue to decrease, and the energy storage modulus decreases more than the dissipation modulus, and the two tend to be close to each other. In the high-strain region, the modulus continues to decrease, and the dissipation modulus is larger than the energy storage modulus, indicating that the viscosity of the material is greater than the elasticity at this time, and the internal structure of the material is completely broken up, reflecting the nature of the liquid. The irregular process of the curve shown in Figure 10 is due to the fact that although the material oscillates at a certain frequency during DSR testing, the homogeneity of CGFB is damaged during the oscillation process, which may result in more irregularity in the modulus change curve. But it can be seen that the modulus decreases with increasing strain. Comparing Figure 10a,c,e, it can be seen that with the increase in cement content, the energy storage modulus and loss modulus of the material have increased, which is because cement as a kind of bonding material has the role of filling the voids and increasing the internal connectivity of the material. As the cement content increases, the connections between cement particles are enhanced, filling the microscopic pores of the material, thus increasing the energy storage modulus and dissipation modulus of the material. High cement content allows more cement particles to fill the pores, thus increasing the energy storage modulus and dissipation modulus of the material. In addition, the hydration reaction of cement in water forms a cement gel, which increases the cohesion and hardness of the material, thus increasing the energy storage modulus and dissipation modulus, and the addition of cement changes the microstructure of the filling slurry, making the material more compact. The increase in cement content has a significant effect on the energy storage modulus and dissipation modulus of the filling slurry, which is mainly due to the filling effect of cement, the hydration reaction of cement, and the change in the microstructure of the material.

Tan delta is defined as the phase angle tangent, which means the ratio of loss modulus to energy storage modulus. The magnitude of the phase angle can be used to visualize the viscoelastic change of the material. It can be seen from Figure 10b,d,f that in the low strain region, the phase angle tangent is small and constant, which indicates that the solid-like elasticity exhibited by the slurry is the main property of the material when it starts to undergo the flow change, and at this time, the embodied yield stress is the stress level at which the material starts to undergo an observable nonlinear deformation, which is usually regarded as the critical point at which the material begins to flow or undergoes plastic deformation. Therefore, the energy storage modulus is higher than the loss modulus in the early stage, reflecting the solid-like nature. The value of the energy storage modulus is usually related to the yield stress of the material because a higher energy storage modulus means that the material is more capable of storing energy when stressed and thus exhibits higher yield stress. In the medium strain region, with the increase in strain, the internal structure of the material is broken, and the orderly linkage formed between the particles is interrupted. At this time, part of the energy applied to the material from outside is converted into elastic energy and stored, while part of it is released as dissipated energy, and the tangent of the phase angle is seen to be increased, which indicates that the percentage of the dissipated energy is increased at this time, and the particles and the slurry within the material are further reorganized. In the high-strain region, due to the further action of the shear force, the dissipative energy increases, and the internal structure changes lead to a reduction in its elasticity, which reflects the viscosity of the material at this time. When a material has a high percentage of dissipative modulus, it means that it loses more energy when subjected to force, which may be related to the fact that it exhibits greater viscosity.

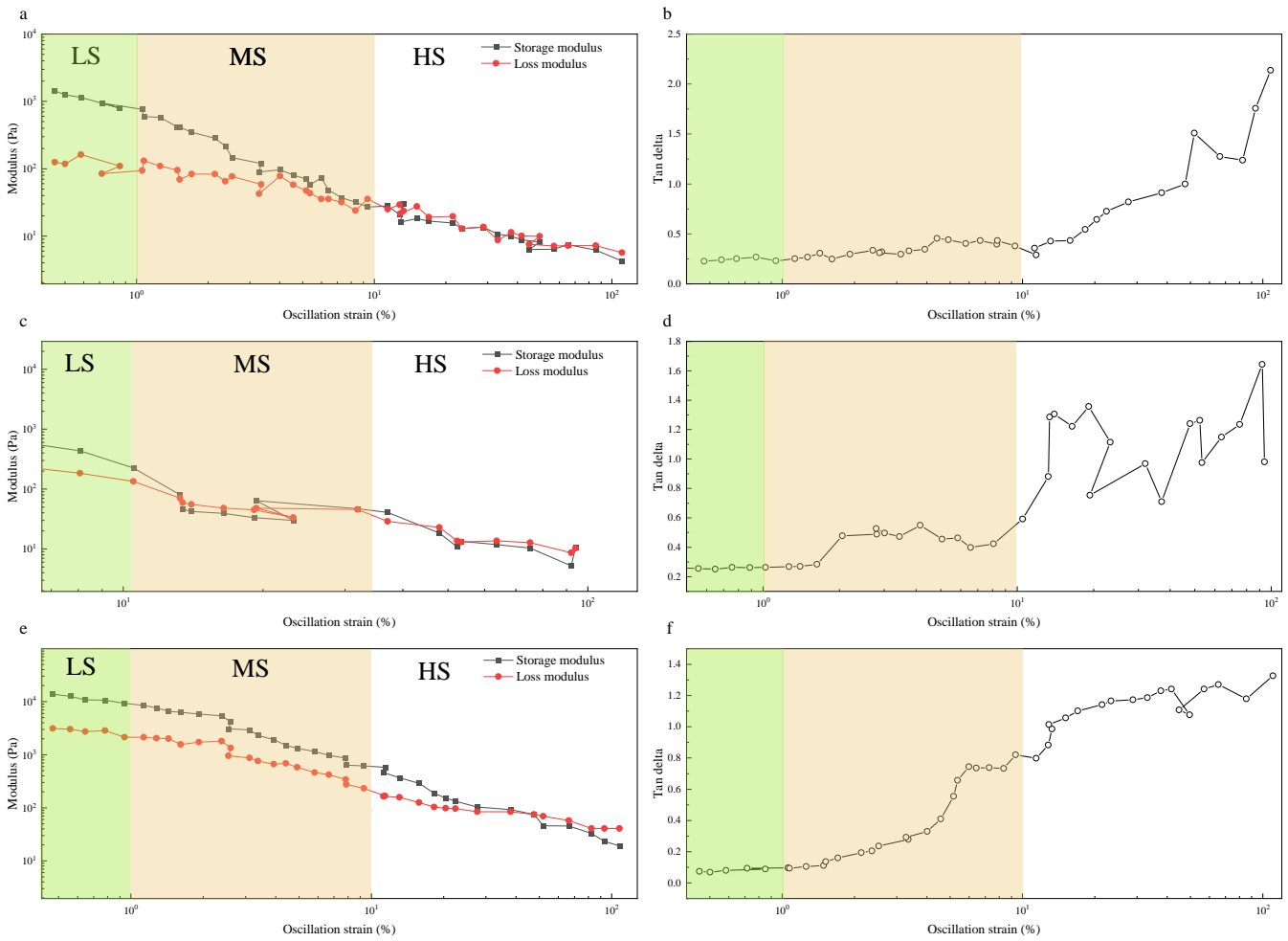


Figure 10. Viscoelastic parameters and phase angle of CGFB ((a,b)-cc8, (c,d)-cc12, (e,f)-cc16).

3.3. Electrical Resistivity Test Results

The results of the resistivity tests of the three raw materials are shown in Figure 11, and it is evident that fly ash and gangue have substantially higher resistivity than cement. Meanwhile, from the resistivity test of different solid concentrations in Figure 12, it can be seen that with the increase in concentration, the resistivity of the material shows an increasing trend, because the test solution is homogeneously stirred and centrifuged after the test results, so it can be concluded that the ions in the slurry carried out a full reaction and combination. The growth rate of resistivity from SC72-SC76 at the moment of 0 is 2.48%, 6.63%, 6.41%, and 4.11% in that order, with a total growth rate of 21.05%. With time, resistivity shows a downward trend, specifically manifested in each group of data at the end of the test to obtain the resistivity, and the initial moment of the decline of 13%–17%, due to the mixing process over time being broken up by the conductive ions for precipitation and new combinations, resulting in a decline in resistivity. The electrical resistivity at time 0 can determine the variation pattern of the viscosity and plasticity of the slurry obtained from the visco-plasticity test. After 55 min, as the electrical resistivity tends to stabilize, the measured electrical resistivity can show the stability and degree of segregation of the internal structure of the slurry during the flow process. Gangue cemented filling material is a non-homogeneous composite material. The type, content, and particle size distribution of the raw material will have a greater impact on the resistivity of the slurry [33]. The resistivity of large particles in gangue is much larger than that in other fine aggregates. The transport of ions is dominated by the pathways within the CGFB slurry [34,35]. It can be seen that the resistivity of CGFB slurry before solidification is mainly determined by the resistivity of fine gangue slurry in the liquid phase. The main components of cement,

fly ash, and gangue in the fine gangue slurry are oxidized minerals and silicate minerals, which are ion-conducting minerals, and their charge carriers are ions. The resistivity of fine gangue slurry is mainly determined by the type of ions, the concentration of ions, the tortuosity of the ion transmission path, and the ion flux area. Among them, the type of ions depends on the chemical composition of raw materials; the concentration of ions depends on the content of raw materials, the degree of solubility of soluble ions and minerals, and the degree of hydration reaction; the tortuosity of the ion transmission path and the ion flux area depends on the content of coarse aggregate. As the concentration increases, there are fewer pathways available for ion exchange per unit volume, so this leads to an increase in resistivity.

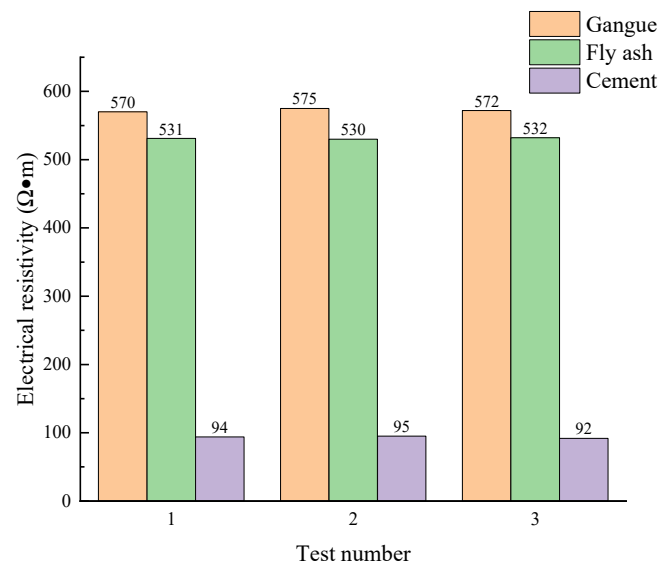


Figure 11. Raw material resistivity.

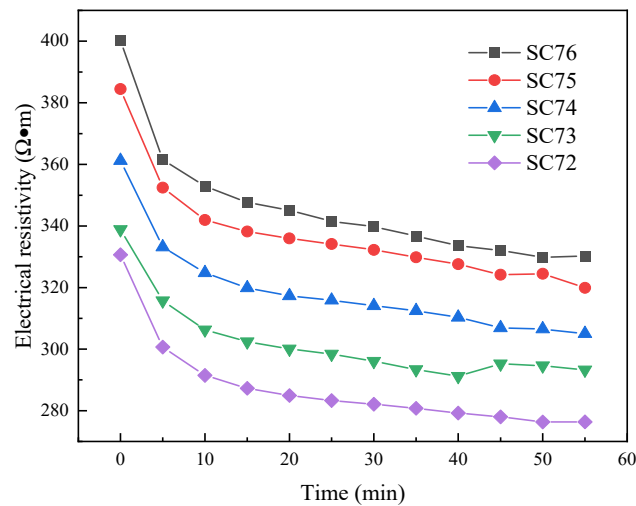


Figure 12. Resistivity at different solid concentrations.

It can be seen in Figure 13 that in CGFB slurry, resistivity usually shows a decreasing trend with increasing cement content. This trend can be explained by several factors. Firstly, cement, as a cementitious material, has a higher electrical resistivity compared to gangue and fly ash. As the cement content increases, there are more cement particles in the filling slurry, the contact area between the cement particles increases, and the conductive paths become more continuous. These conductive paths provide channels for the transport of electrons and reduce resistivity. Second, the physical and chemical properties of the

filling slurry change when the amount of cement increases. Increasing the cement content may result in increased bonding of the filling slurry and a reduction in the gaps between particles, which reduces the resistivity. In addition, factors such as the shape and size of the cement particles and their distribution may also affect the change in resistivity. Therefore, in CGFB slurries, increasing the cement content usually leads to a decrease in resistivity. However, it should be noted that when the cement content exceeds 12%, the resistivity between the two experimental groups CC14 and CC16 tends to be similar, which is because the filling effect between the cement particles will be saturated, and further increases in the cement content may not significantly reduce the resistivity and may even lead to the trend of resistivity change tending to stabilize. Therefore, in specific research and application, the range of variation in cement content and the combined effect of other influencing factors need to be considered.

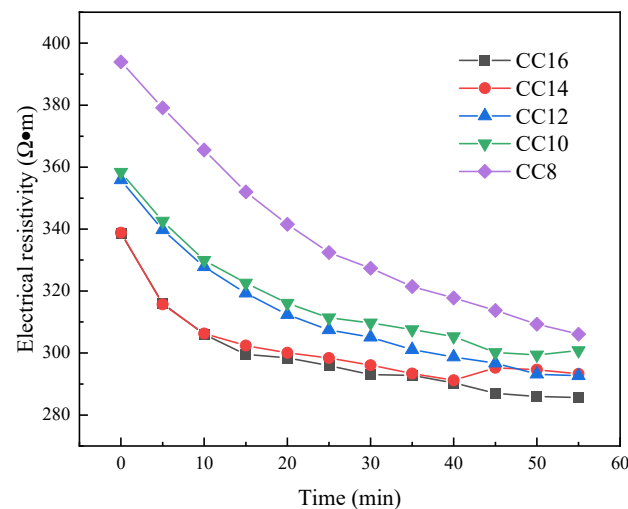


Figure 13. Resistivity at different cement concentrations.

4. Conclusions

In this paper, the viscoelasticity-plasticity of CGFB slurries with varying solid contents and cement dosages was examined, and the yield stress, viscosity, modulus, and resistivity of the materials were tested experimentally. The findings lead to the following conclusions:

1. The concentration of solids has an important effect on the rheological properties of the material. When the solid phase content increases from 72% to 76%, the viscosity and yield stress of the material both increase, and the increase reaches 32.77% and 51.22%, respectively. The reason is that the increase in concentration leads to a decrease in the free water content, which in turn increases the contact area between the particles. With the increase in cement content from 8% to 16%, the yield stress increased by 53.07% and the viscosity increased by 79.78%, which is due to the flocculation and hydration of the cement.

2. The viscoelasticity of the material under the dynamic shear action at the frequency of 1 Hz, the energy storage modulus is greater than the loss modulus in the low-strain region, and the material shows a greater proportion of the elastic nature of the solid, and with the increase in the strain, the energy storage modulus and the dissipation modulus both show a decreasing trend. This is due to the shear damage suffered by the structure inside the pulp. In the high-strain region, the dissipation modulus and energy storage modulus are the same, and the tangent of the phase angle also increases with the increase in strain, indicating that the elasticity of the material gradually decreases and the viscosity increases. With the increase in cement content, the energy storage modulus and dissipation modulus of the material show an increasing trend, which is related to the filling effect of cement, the hydration reaction of cement, as well as the change in the microstructure of the material.

3. Compared to gangue and fly ash, cement has a substantially lower electrical resistance, while the electrical resistivity of CGFB materials shows an increasing trend with increasing solid concentration, with an increase of 21.05% for SC72-76. This is due to the mixing process of ions in the full reaction and binding, resulting in a reduction in ionic pathways in the slurry, which leads to an increase in resistivity. The resistivity is determined by the ion-conducting mineral composition of cement, fly ash, and gangue in the fine gangue slurry, whose charge carriers are ions. As the concentration increases, the decrease in the conductive path leads to an increase in resistivity.

4. In CGFB filling slurry, with the increase in cement content, the resistivity generally shows a downward trend, which is caused by the increase in the electrical resistivity of cement and changes in the physical and chemical properties of the filling slurry. It should be noted that when the cement content exceeds 12%, the resistivity trend may tend to stabilize because the cement filling effect has reached saturation.

Author Contributions: Conceptualization, Y.H.; data curation, B.F. and K.Y.; funding acquisition, C.W., B.F. and K.Y. investigation, Y.H. and X.S; methodology, Y.H.; project administration, B.F.; resources, Y.H. and B.F.; software, Y.H.; supervision, Y.H. and X.S.; validation, C.W., B.F. and K.Y.; visualization, B.F. and C.W.; writing—original draft preparation, Y.H.; writing—review and editing, Y.H., X.S. and C.W. All authors have read and agreed to the published version of the manuscript.

Funding: This research received no external funding.

Data Availability Statement: Data are contained within the article.

Conflicts of Interest: The authors declare no conflicts of interest.

References

1. Yang, B.; Wang, X.; Yin, P.; Gu, C.; Yin, X.; Yang, F.; Li, T. The Rheological Properties and Strength Characteristics of Cemented Paste Backfill with Air-Entraining Agent. *Minerals* **2022**, *12*, 1457. [[CrossRef](#)]
2. Li, B.; Zhang, J.; Yan, H.; Zhou, N.; Li, M. Experimental investigation into the thermal conductivity of gangue-cemented paste backfill in mine application. *J. Mater. Res. Technol.* **2022**, *16*, 1792–1802. [[CrossRef](#)]
3. Zhang, M.; Qiu, Y.; Li, C.; Cui, T.; Yang, M.; Yan, J.; Yang, W. A Habitable Earth and Carbon Neutrality: Mission and Challenges Facing Resources and the Environment in China—An Overview. *Int. J. Environ. Res. Public Health* **2023**, *20*, 1045. [[CrossRef](#)] [[PubMed](#)]
4. Zhu, A.; Wang, Q.; Liu, D.; Zhao, Y. Analysis of the Characteristics of CH₄ Emissions in China's Coal Mining Industry and Research on Emission Reduction Measures. *Int. J. Environ. Res. Public Health* **2022**, *19*, 7408. [[CrossRef](#)] [[PubMed](#)]
5. Bo, L.; Yang, S.; Liu, Y.; Zhang, Z.; Wang, Y.; Wang, Y. Coal Mine Solid Waste Backfill Process in China: Current Status and Challenges. *Sustainability* **2023**, *15*, 13489. [[CrossRef](#)]
6. Qi, T.; Gao, X.; Feng, G.; Bai, J.; Wang, Z.; Chen, Q.; Wang, H.; Du, X. Effect of biomass power plant ash on fresh properties of cemented coal gangue backfill. *Constr. Build. Mater.* **2022**, *340*, 127853. [[CrossRef](#)]
7. Wu, J.; Liu, X. Risk assessment of underground coal fire development at regional scale. *Int. J. Coal Geol.* **2011**, *86*, 87–94. [[CrossRef](#)]
8. Wang, Y.; Zhang, X.; Sugai, Y.; Sasaki, K. A Study on Preventing Spontaneous Combustion of Residual Coal in a Coal Mine Goaf. *J. Geol. Res.* **2015**, *2015*, 712349. [[CrossRef](#)]
9. Zhang, X.; Feng, X.; Wang, Z.; Jian, J.; Chen, S.; Luo, W.; Zhang, C. Experimental study on the physico-mechanical properties and microstructure of foam concrete mixed with coal gangue. *Constr. Build. Mater.* **2022**, *359*, 129428. [[CrossRef](#)]
10. Wu, D.; Sun, G.; Liu, Y. Modeling the thermo-hydro-chemical behavior of cemented coal gangue-fly ash backfill. *Constr. Build. Mater.* **2016**, *111*, 522–528. [[CrossRef](#)]
11. Wu, D.; Yang, B.; Liu, Y. Transportability and pressure drop of fresh cemented coal gangue-fly ash backfill (CGFB) slurry in pipe loop. *Powder Technol.* **2015**, *284*, 218–224. [[CrossRef](#)]
12. Wang, X.; Zhao, B.; Zhang, C.; Zhang, Q. Paste-like self-flowing transportation backfilling technology based on coal gangue. *Min. Sci. Technol.* **2009**, *19*, 137–143. [[CrossRef](#)]
13. Haiqiang, J.; Fall, M.; Cui, L. Yield stress of cemented paste backfill in sub-zero environments: Experimental results. *Miner. Eng.* **2016**, *92*, 141–150. [[CrossRef](#)]
14. Sun, K.; Zhang, J.; He, M.; Li, M.; Guo, S. Control of surface deformation and overburden movement in coal mine area by an innovative roadway cemented paste backfilling method using mining waste. *Sci. Total Environ.* **2023**, *891*, 164693. [[CrossRef](#)]
15. Shi, Z.; Zhao, H.; Liang, B.; Sun, W.; Wang, J.; Fang, S. Simulation test study on filling flow law of gangue slurry in goaf. *Sci. Rep.* **2023**, *13*, 19117. [[CrossRef](#)] [[PubMed](#)]
16. Min, C.; Shi, Y.; Lu, X.; Liu, Z.; Zhou, Y. Cemented backfill using Ca(OH)₂-pretreated phosphogypsum as aggregate: Hydration characteristics, structural features and strength development. *Constr. Build. Mater.* **2023**, *402*, 133011. [[CrossRef](#)]

17. Zhao, X.; Yang, K.; Wei, Z.; He, X.; Chen, R. Study on the effect of multi-source solid waste on the performance of its backfill slurry. *Heliyon* **2023**, *9*, e16251. [[CrossRef](#)] [[PubMed](#)]
18. Yang, J.; Yang, B.; Yu, M. Pressure Study on Pipe Transportation Associated with Cemented Coal Gangue Fly-Ash Backfill Slurry. *Appl. Sci.* **2019**, *9*, 512. [[CrossRef](#)]
19. Rovnanik, P.; Kusák, I.; Bayer, P.; Schmid, P.; Fiala, L. Comparison of electrical and self-sensing properties of Portland cement and alkali-activated slag mortars. *Cem. Concr. Res.* **2019**, *118*, 84–91. [[CrossRef](#)]
20. Mohammed, A.S. Vipulanandan models to predict the electrical resistivity, rheological properties and compressive stress-strain behavior of oil well cement modified with silica nanoparticles. *Egypt. J. Pet.* **2018**, *27*, 1265–1273. [[CrossRef](#)]
21. Wang, Z.H.; Qi, T.Y.; Feng, G.R.; Bai, J.W.; Pei, X.M.; Cui, B.Q.; Song, C.; Ran, H.Y. Electrical resistivity method to appraise static segregation of gangue-cemented paste backfill in the pipeline. *Int. J. Pres. Ves. Pip.* **2021**, *192*, 104385. [[CrossRef](#)]
22. Liu, J.; Zha, F.; Xu, L.; Kang, B.; Tan, X.; Deng, Y.; Yang, C. Mechanism of stabilized/solidified heavy metal contaminated soils with cement-fly ash based on electrical resistivity measurements. *Measurement* **2019**, *141*, 85–94. [[CrossRef](#)]
23. Medeiros-Junior, R.A.; Lima, M.G. Electrical resistivity of unsaturated concrete using different types of cement. *Constr. Build. Mater.* **2016**, *107*, 11–16. [[CrossRef](#)]
24. van Noort, R.; Hunger, M.; Spiesz, P. Long-term chloride migration coefficient in slag cement-based concrete and resistivity as an alternative test method. *Constr. Build. Mater.* **2016**, *115*, 746–759. [[CrossRef](#)]
25. Yim, H.J.; Bae, Y.H.; Jun, Y. Hydration and microstructural characterization of early-age cement paste with ultrasonic wave velocity and electrical resistivity measurements. *Constr. Build. Mater.* **2021**, *303*, 124508. [[CrossRef](#)]
26. Xu, W.; Tian, X.; Cao, P. Assessment of hydration process and mechanical properties of cemented paste backfill by electrical resistivity measurement. *Nondestruct. Test. Eva.* **2018**, *33*, 198–212. [[CrossRef](#)]
27. Xu, W.; Tian, X.; Wan, C. Prediction of Mechanical Performance of Cemented Paste Backfill by the Electrical Resistivity Measurement. *J. Test. Eval.* **2018**, *46*, 2450–2458. [[CrossRef](#)]
28. Feng, G.; Wang, Z.; Qi, T.; Du, X.; Guo, J.; Wang, H.; Shi, X.; Wen, X. Effect of velocity on flow properties and electrical resistivity of cemented coal gangue-fly ash backfill (CGFB) slurry in the pipeline. *Powder Technol.* **2022**, *396*, 191–209. [[CrossRef](#)]
29. Fu, Z.; Li, H.; Deng, J.; Qiao, D.; Wang, J. Bivariate rheological model of ultrafine tailings backfill slurry based on structural parameter and its applications. *Chin. J. Nonferrous Met.* **2021**, *31*, 1672–1685. [[CrossRef](#)]
30. Deng, X.; Klein, B.; Tong, L.; de Wit, B. Experimental study on the rheological behavior of ultra-fine cemented backfill. *Constr. Build. Mater.* **2018**, *158*, 985–994. [[CrossRef](#)]
31. Yin, S.; Shao, Y.; Wu, A.; Wang, Z.; Yang, L. Assessment of expansion and strength properties of sulfidic cemented paste backfill cored from deep underground stopes. *Constr. Build. Mater.* **2020**, *230*, 116983. [[CrossRef](#)]
32. Chidiac, S.E.; Mihaljevic, S.N.; Krachkovskiy, S.A.; Goward, G.R. Characterizing the effect of superabsorbent polymer content on internal curing process of cement paste using calorimetry and nuclear magnetic resonance methods. *J. Therm. Anal. Calorim.* **2021**, *145*, 437–449. [[CrossRef](#)]
33. Yang, L.; Wang, H.; Li, H.; Zhou, X. Effect of High Mixing Intensity on Rheological Properties of Cemented Paste Backfill. *Minerals* **2019**, *9*, 240. [[CrossRef](#)]
34. Gürer, C.; Düşmez, C.; Boğa, A.R. Effects of different aggregate and conductive components on the electrically conductive asphalt concrete's properties. *Int. J. Pavement Eng.* **2023**, *24*, 2068547. [[CrossRef](#)]
35. Rahman, M.L.; Ceylan, H.; Kim, S.; Taylor, P.C. Influence of electrode placement depth on thermal performance of electrically conductive concrete: Significance of threshold voltage for long-term stability. *Constr. Build. Mater.* **2024**, *412*, 134883. [[CrossRef](#)]

Disclaimer/Publisher's Note: The statements, opinions and data contained in all publications are solely those of the individual author(s) and contributor(s) and not of MDPI and/or the editor(s). MDPI and/or the editor(s) disclaim responsibility for any injury to people or property resulting from any ideas, methods, instructions or products referred to in the content.